Materials and Design 56 (2014) 193–199

Contents lists available at ScienceDirect

Materials and Design

journal homepage: www.elsevier.com/locate/matdes

Tensile properties of fiber laser welded joints of high strength low alloy and dual-phase steels at warm and low temperatures

D. Parkes [a], D. Westerbaan [b], S.S. Nayak [b], Y. Zhou [b], F. Goodwin [c], S. Bhole [a], D.L. Chen [a,*]

[a] Department of Mechanical and Industrial Engineering, Ryerson University, 350 Victoria Street, Toronto, Ontario M5B 2K3, Canada
[b] Department of Mechanical and Mechatronics Engineering, University of Waterloo, 200 University Avenue West, Waterloo, Ontario N2L 3G1, Canada
[c] International Zinc Association, Durham, NC 27713, USA

ARTICLE INFO

Article history:
Received 27 August 2013
Accepted 30 October 2013
Available online 9 November 2013

Keywords:
Fiber laser welding
Dissimilar joint
High strength low alloy steel
Dual-phase steel
Tensile
Temperature

ABSTRACT

High strength low alloy (HSLA) and dual-phase DP980 (UTS ⩾ 980 MPa) steels were joined using fiber laser welding in similar and dissimilar materials combinations. The welded joints were characterized with respect to microhardness and tensile properties at three different temperatures: −40 °C, 25 °C, and 180 °C. Tensile properties of the welded joints were compared to those of the base metal (BM) obtained under similar conditions. A good correlation was found between the welded joints and the BM in relation to the tensile properties obtained at the different temperatures. A general trend of increase in the yield strength (YS), the ultimate tensile strength (UTS) and energy absorption (EA) with decreasing temperature was observed; however, work hardening coefficient was not altered and insignificant scatter was observed in case of the elongation. However, in the DP980 steel, dynamic strain ageing was observed only in the BM.

1. Introduction

In order to reduce the volume of CO_2 emission into the atmosphere, a significant increase in the fuel efficiency of the vehicles is required [1–3]. Therefore, automotive manufacturers are continuously looking for methods to achieve this goal. One of the popular methods to increase the fuel efficiency is to use the auto-body parts made of stronger materials, which will help in down-gauging leading to decrease in the vehicle weight [2,3]. Advanced high strength steel (AHSS) is a family of such materials, thinner sheets of which can replace conventional thicker materials used in auto-body structures i.e. low carbon steel, interstitial free steel or high strength low alloy steel (HSLA) steel, without compromising crash-worthiness because of their higher strength and good formability [4–6]. Dual phase (DP) steel is one of the popular AHSS that is being increasingly used in the automotive industries [6]. Currently, several grades of DP steel are being considered for certain parts of auto-body where higher strength is necessary, e.g., B-pillars and bumpers [7] that were previously made of HSLA steel.

Welding is the primary joining process in automotive industry; therefore, lots of work has been done on the weldability, microstructure, and performance of AHSS in order to determine their implementation in current and future cars [8–13]. CO_2, Nd:YAG, and recently fiber laser are used for manufacturing laser welded blanks (LWBs), also known as tailor welded blanks, which are formed into different required three dimensional auto-body parts [14]. Among all laser welding processes, fiber laser welding (FLW) has been shown recently [8–10] to provide improved tensile and fatigue properties for the DP980 steel welded joints because of the possibility to reduce the size of the weld zones. In addition, FLW has several other advantages e.g. smaller beam size, lower maintenance costs, higher efficiency, high precision and reliability, and low space requirements due to compact design [14]. Considering the applicability in the auto industry, several studies have been done in last decades to investigate the effects of different welding processes on the microstructure and mechanical properties of the DP steel welded joints [8–12]. A common conclusion, which all these studies reported, was the softening, which occurs in the sub-critical heat affected zone (HAZ) where temperature experienced by the work piece is close to or below Ac_1 line [8–13]. Softening is associated with tempering of the martensite leading to a drop in the hardness below that of the base metal (BM) [8–10,12,13] and deterioration in the performance of the DP steel welded joints [8–13].

Although DP steels are emerging candidates, the major parts of the cab body are still dominated by HSLA steel. Considering this, researchers have been interested in and studied the microstructure and mechanical properties of the similar and dissimilar welded joints between HSLA and DP980 steels [8–13]. There are also reports on the effects of temperature on the mechanical properties of DP980 steels [15–20]. However, there is no report on the

* Corresponding author. Tel.: +1 416 979 5000x6487; fax: +1 416 979 5265.
E-mail address: dchen@ryerson.ca (D.L. Chen).

0261-3069/$ - see front matter © 2013 Elsevier Ltd. All rights reserved.
http://dx.doi.org/10.1016/j.matdes.2013.10.087

Table 1
Chemical composition of the DP980 and HSLA steel investigated (wt.%).

Steel	C	Mn	Si	Al	Cr	Ni	N	Fe
DP980	0.15	1.45	0.33	0.05	0.02	0.01	0.009	Balance
HSLA	0.08	0.83	0.5	0.05	0.03	0.01	0.007	Balance

mechanical behavior of the welded joints of HSLA and DP980 steels at low and warm temperatures, which is important to investigate considering the environmental conditions to which vehicles are exposed. The present study was carried out to fill the gap in the literature and reports the mechanical properties of the fiber laser welded joints of DP980 and HSLA steels in similar and dissimilar materials combinations evaluated at cryogenic, room and elevated temperatures.

2. Experimental procedure

Hot dip galvanized (GI) sheets of DP980 and HSLA steels with a thickness of 1.2 mm were used in this study. The chemical compositions and the microstructure of the steels are given in Table 1 and Fig. 1, respectively. HSLA contained a fine grained ferritic matrix dispersed with ultra-fine alloyed carbides. DP steels have a ferritic matrix embedded with islands of martensite (~56%).

The steel sheets were sheared into 100 mm × 200 mm coupons, which had the sheared edges placed together for running welds in butt joint configuration to make 200 mm × 200 mm LWBs, as shown in Fig. 2(a). Welding was done perpendicular to the rolling direction of the sheets in an IPG Photonics YLS-6000 fiber laser system using a power and speed of 6 kW and 16 m/min, respectively. The laser had a beam focal length of 20 cm, and a spot size of 0.6 mm. The core diameter of the fiber laser was 0.3 mm. Welding was performed with a head angle of 0° and no shielding gas was used during the welding process [13].

Microstructure study was done on the weld cross-sections, which were prepared following standard metallographic procedure e.g. mounting, grinding, polishing using 1 μm diamond suspension followed by etching with 2% Nital solution. The optical microscopy and scanning electron microscopy (SEM) study on the etched specimens was performed using a Nikon Epiphot light microscope equipped with Clemex image analysis software and JEOL JSM-6380 scanning electron microscope equipped with Oxford energy dispersive X-ray spectroscopy (EDS), respectively. Etched specimens were also used to obtain the Vickers microhardness profiles across the welded joints using a Buehler micromet 5103 computerized microhardness tester using a 200 g load for 15 s dwell time. The microhardness indentations were spaced sufficiently apart to prevent interference from the localized strain hardening from the adjacent indentations. To ensure the validity of the microhardness measurements, calibration was done on a standard specimen.

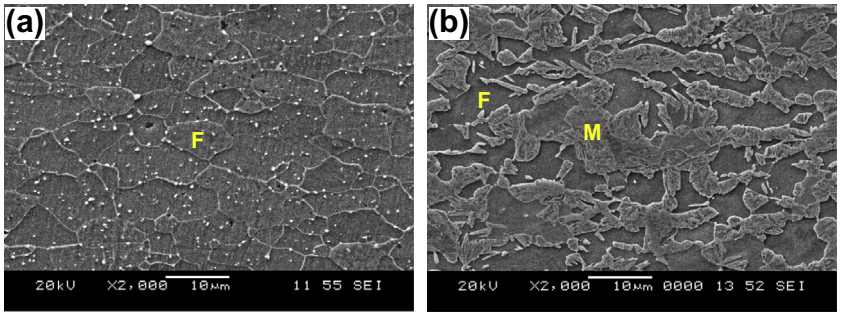

Fig. 1. Microstructure of HSLA-DP980 weld at RT (a) HSLA BM, (b) DP980 BM. (F: ferrite, M: martensite).

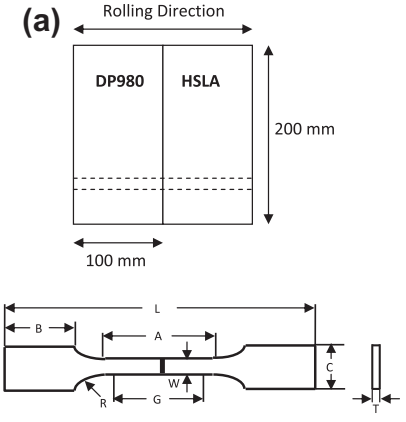

(b)

Position	G	W	R	L	A	B	C	T
Dimension (mm)	50	12.5	12.5	200	57	50	20	1.2

Fig. 2. Schematic diagram illustrating (a) the gometry of the fiber laser welded joint, (b) a transverse tensile specimen of the FLWedweld obtained machinedalong the dashed lines in (a).

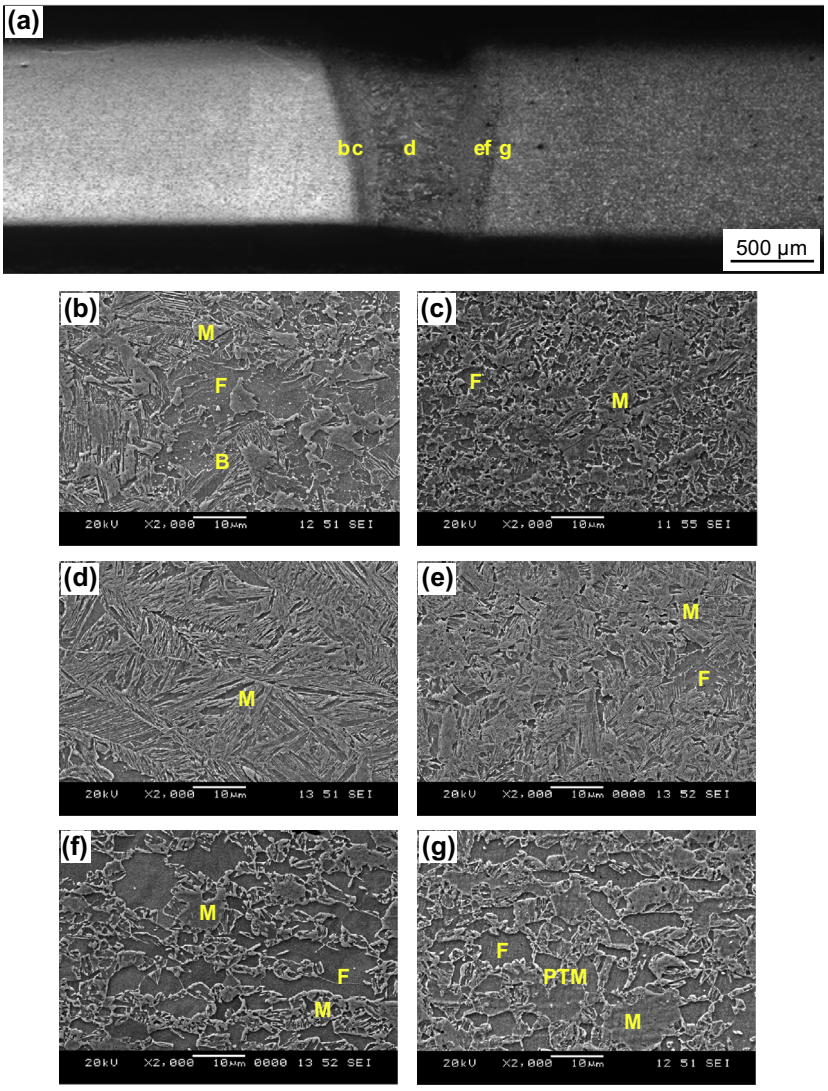

Fig. 3. Microstructure of HSLA-DP980 weld at RT (a) Overview of the dissimilar weld, (b) HSLA intercritical HAZ, (c) HSLA upper critical HAZ, (d) FZ, (e) DP980 upper critical HAZ, (f) DP980 intercritical HAZ and (g) DP980 subcritical HAZ. (F: ferrite, M: martensite, B: bainite, PTM: partially tempered martensite).

Transverse tensile test samples following ASTM: E8/E8 M standard were machined from the welded blanks, as indicated by the dashed line in Fig. 2(a). The dimensions of the specimens used are shown in Fig. 2(b). The samples were machined in such a way that the weld was positioned at the center of gauge length (Fig. 2(b)). Tensile tests were conducted using a strain rate of $1 \times 10^{-3}\ s^{-1}$ at three different temperatures until rupture. A fully computerized United tensile testing machine was used for room temperature (RT, 25 °C) testing whereas for low temperature (LT, −40 °C) and high temperature (HT, 180 °C) tests a United environmental chamber controller with a tolerance of ±5.5 °C was used. These temperatures were chosen in order to represent cold winter weather and a hot car engine condition. For low and high temperature tests, the samples were cooled or heated within the chamber without any load to allow possible change in dimensions before the tests. An extensometer with a gauge length of 25 mm and a strain limit of 20% was used to measure the strain during the tensile tests and at least two specimens were tested at each temperature.

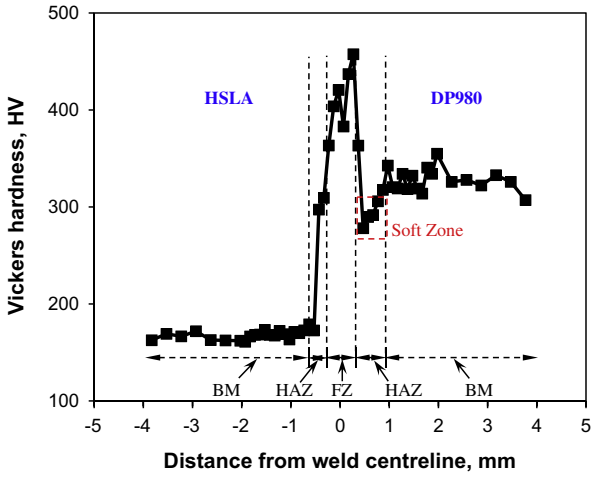

Fig. 4. Microhardness profile of FLW HSLA-DP980 sample.

3. Results and discussion

3.1. Microstructure evolution

The profile and the microstructure of the different zones of the dissimilar DP980-HSLA welded joints are shown in Fig. 3. The

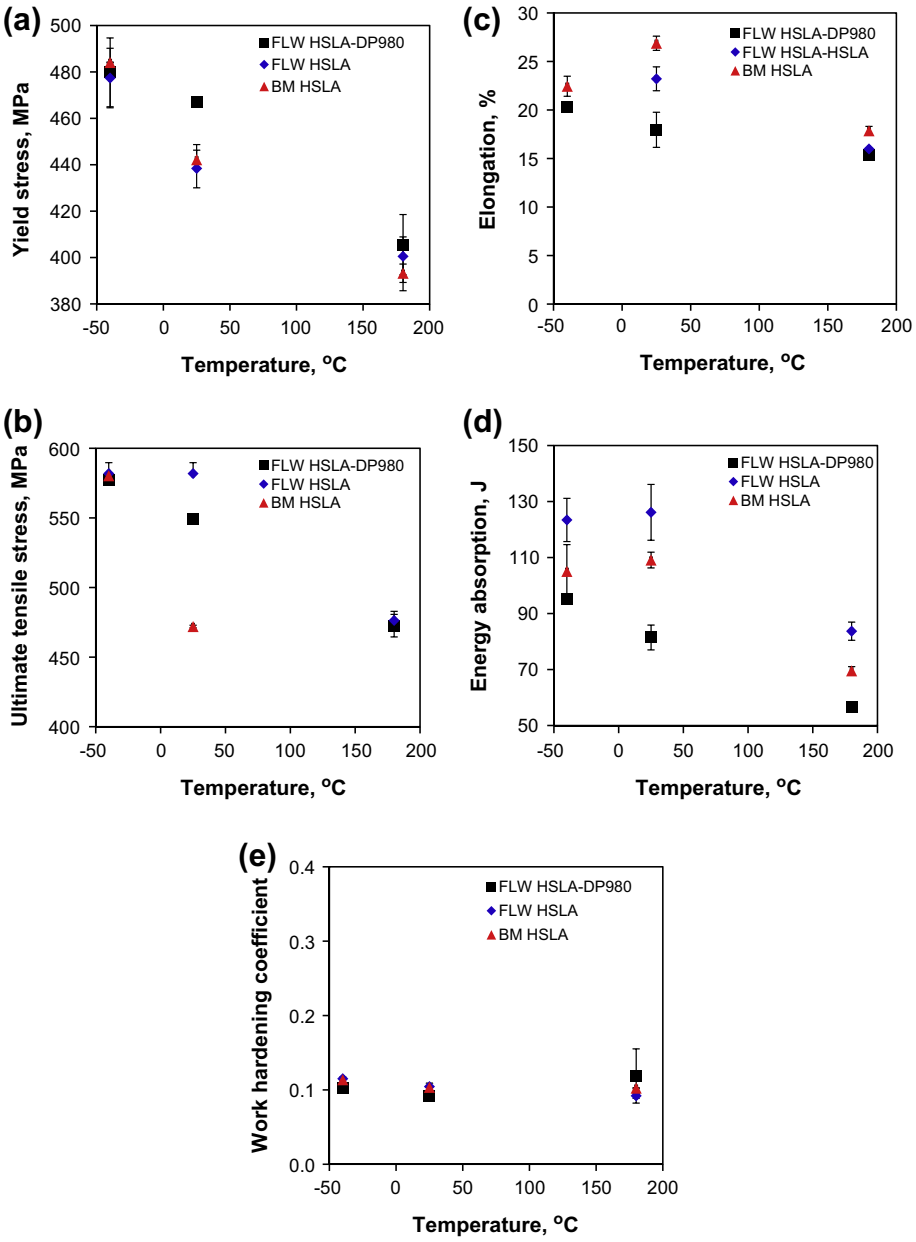

Fig. 5. Comparison of tensile properties of the HSLA BM, HSLA-DP980 and HSLA–HSLA welded joints at different temperatures: (a) YS, (b) UTS, (c) elongation, (d) EA and (e) work hardening coefficient.

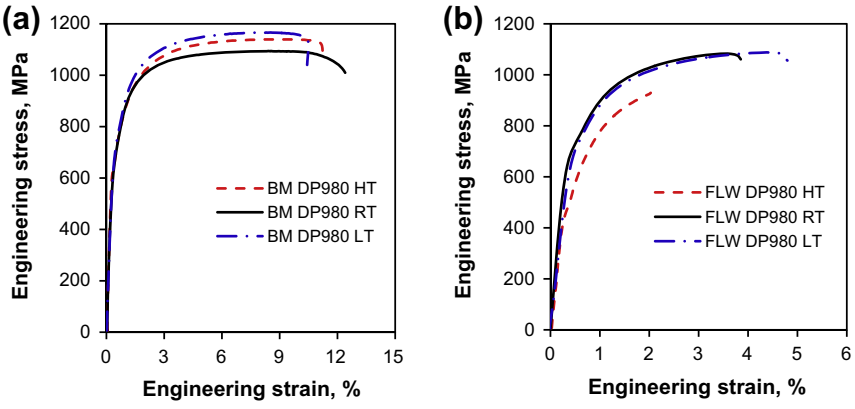

Fig. 6. Typical tensile curves of (a) DP980 BM and (b) DP980–DP980.

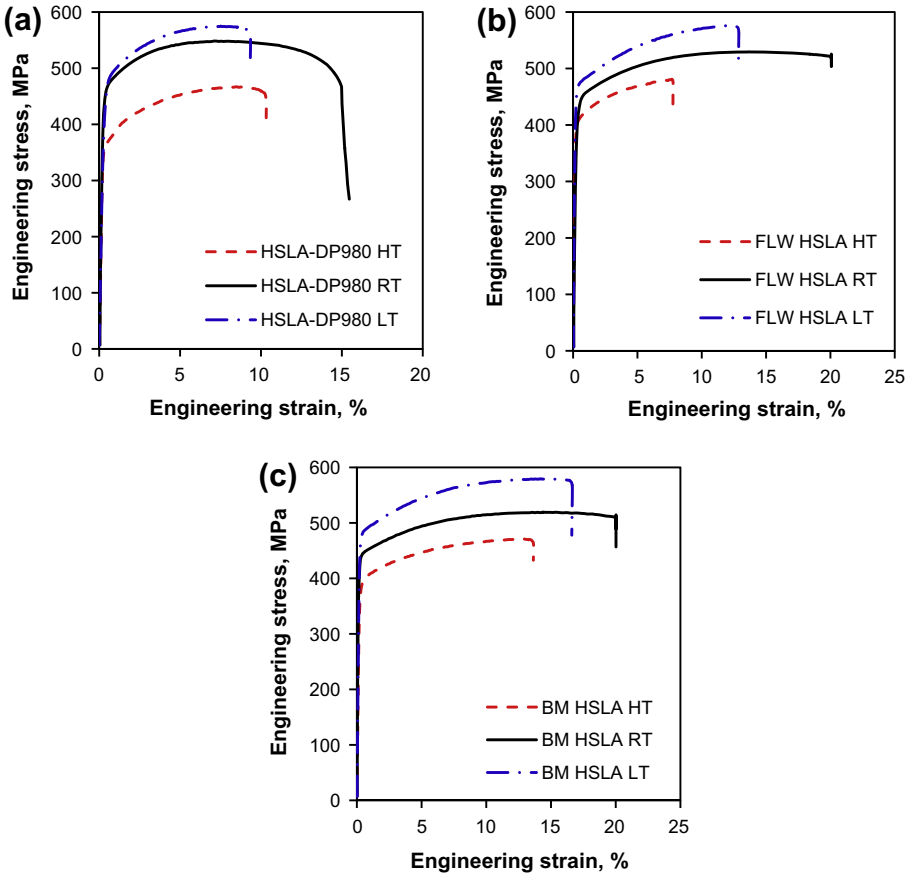

Fig. 7. Typical tensile curves of (a) HSLA-DP980, (b) HSLA–HSLA and (c) HSLA BM.

fusion zone (FZ) showed a single phase martensitic structure (Fig. 3(d)), which is because of the rapid cooling rate generated by the high welding speed. The regions next to either side of the FZ are the HAZ where the materials were not melted but still experienced high temperatures. The HAZ contained different sub-regions, the upper-critical HAZ, the inter-critical HAZ, and the sub-critical or partially tempered HAZ [8–13]. On the HSLA steel side of the welds, the upper-critical HAZ (Fig. 3(c)) exhibited a highly martensitic microstructure with little fraction of ferrite phase due to the fact that during the welding process the temperature of that region is between the Ac_3 line and the melting temperature of steel. Because of this, a significant portion of the microstructure transformed into austenite which upon rapid cooling involved in FLW transformed back to martensite. In the inter-critical HAZ zone the temperature experienced by the materials was between the Ac_1 and Ac_3 lines; this caused the microstructure to be partially transformed into austenite upon heating which during cooling formed martensite and bainite with the untransformed ferrite matrix (Fig. 3(b)). On the DP980 side of the dissimilar weld, the upper-critical HAZ showed a microstructure similar to the HSLA side of the weld having dominantly martensite phase (Fig. 3(e)). The inter-critical HAZ (Fig. 3(f)) has a microstructure similar to the BM (Fig. 1(b)) containing ferrite and martensite phases. The sub-critical HAZ or the soft zone (Fig. 3(g)) was formed because the temperature in this region reached close to or below the A_{C1} line, which caused the metastable martensite in the BM to decompose to form partially tempered martensite (PTM) [13].

3.2. Microhardness

The microhardness profile of the dissimilar DP980-HSLA welded joint clearly showed the different regions and sub-regions formed after FLW (Fig. 4). Similar materials made under the same conditions have also been shown in Parkes et al. [13]. The HSLA BM due to its soft and ductile matrix has a lower mean hardness of 168 VHN. In the HAZ on the HSLA side, no softening was observed and a sharp increase in hardness was observed due to formation of harder phases e.g. martensite and bainite the fraction of which increases with distance from the BM toward the FZ. Interestingly, two sub-regions within the FZ were observed as indicated by the two different peaks in the hardness profile. This is attributed to the rapid cooling rate achieved in the FZ because of the high welding speed (16 m/min). The process was so fast that there was no time for the diffusion to occur during cooling, which led to chemical inhomogeneity within the FZ resulting in different hardness i.e. two distinct peaks, which was also seen in Parkes et al. [13]. The upper critical HAZ on the DP980 side of the welded joint was found to be similar to that on the HSLA side and the inter-critical HAZ on the DP980 side contains newly formed martensite and ferrite like its BM contributing to higher hardness compared to HSLA. A significant drop in the hardness was observed at the outer HAZ (251 VHN) compared to the BM (326 VHN), which is due to the decomposition of martensite to form soft ferrite phase along with precipitated carbides [8–13].

3.3. Tensile properties

The comparison of the YS, UTS, elongation, EA, and the work hardening coefficient obtained at different test temperature for the HSLA BM, HSLA-DP980 and HSLA–HSLA welded joints is shown in Fig. 5. It should be noted that the EA was obtained by calculating the area under the load–displacement curves obtained from the tensile tests. Tensile properties were found to decrease with increasing temperature in all the specimens (Fig. 5).

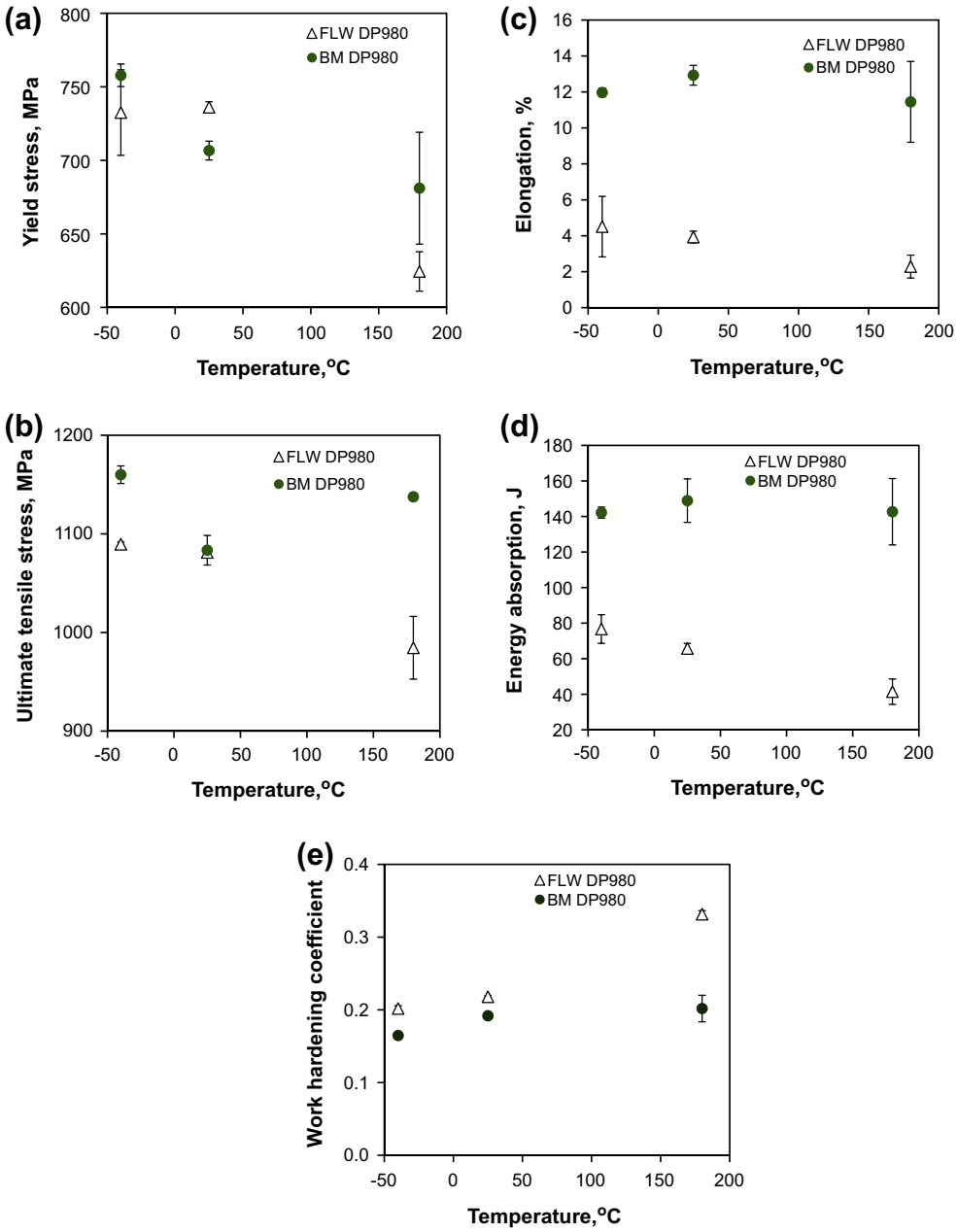

Fig. 8. Comparison of tensile properties of the DP980 FLWed joints and the BM tested at different temperatures: (a) YS, (b) UTS, (c) elongation, (d) energy absorbed and (e) work hardening coefficient.

Corollary to Parkes et al. [13], only the HSLA side of the HSLA-DP980 welded joint is deformed during loading because of the lower strength HSLA side compared to even the soft zone present on the DP980 side of the welded joint (Fig. 4). Chen et al. [21] also showed the decrease in the mechanical properties of HSLA steels at higher temperatures and whose results fell closely with this study; the UTS and YS decreased with temperature which in turn decreased the EA since the elongation of the samples remained relatively constant at all temperature (Fig. 5c) [22,23]. The Holloman equation, Eq. (1) [24], models the plastic behavior on a true stress true strain tensile curve up to the UTS, where σ_T is the true stress, K is the strength coefficient, ε_T is the true strain, and n is the work hardening coefficient. The higher the work hardening coefficient, the more hardening is occurring; for the HSLA containing samples, the work hardening coefficient remained relatively constant over the different temperatures which was reflected from the stress–strain curve showing little alteration in the shape of the plastic region (Figs. 6 and 7). The trend in the change of properties of the HSLA BM and the welds (HSLA–HSLA and HSLA-DP980) was observed as a function of temperature within normal scatter.

$$\sigma_T = K\varepsilon_T^n \tag{1}$$

The tensile results of DP980 BM and the DP980–DP980 welded joints at different test temperatures are summarized in Fig. 8. Examining the trends reveals interesting information about the properties of the DP980 welded joints in comparison to the BM properties; the most obvious difference is in the UTS. It was found that in the DP980 welded joint there is a consistent decrease in the strength with increasing temperature, which could be attributed to the higher mobility of dislocations allowing for dislocation climb [22,23]. This increased deformation caused the soft zone in the

HAZ to have a greater effect and to fail at a lower stress. However, in the DP980 BM there was a decrease in UTS from −40 °C to 25 °C with an increase in the UTS from 25 °C to 180 °C. This increase in strength with temperature above room temperature has been reported in literature [20,21,25] as dynamic strain aging (DSA), which occurs when the dislocations are temporarily arrested by solute carbon and nitrogen atoms, which inhibits further movement of the dislocation and subsequently requires more stress to overcome the obstacles thus increasing the strength [16–20,21,25]. The YS of both the DP980 BM and the welded joint showed a decreasing trend with increasing temperature, which can be related to the kinetic vibrations in the lattice and how easily the dislocations can move in it [22,23]. Both elongation and EA remained relatively consistent over all temperatures for the DP980 BM due to the high strength of the material; however, the elongation of the DP980–DP980 welded joint was found to be much less in comparison to it BM at -all temperatures (Figs. 6 and 8(c)) which is why the EA of the welded joint is significantly less than that of the BM (Fig. 8(d)). Lastly, the work hardening coefficient was not observed to change with temperature for the DP980 BM since the shape of the stress–strain curve did not undergo significant changes in shape (Fig. 6(a)); however, the DP980–DP980 welded joint at 180 °C showed an apparent increase in the work hardening coefficient caused by a change in shape of its stress–strain curve (Fig. 6(b)) where there is a decrease in both the elongation and strength. This shortening and lowering of the stress–strain curve (lower strength and ductility) causes this apparent increase of the work hardening coefficient.

4. Conclusion

The mechanical properties of the fiber laser welded joints of DP980 and HSLA steels in similar and dissimilar materials combinations evaluated at cryogenic, room, and elevated temperatures showed the following:

(1) In both similar and dissimilar welded specimens there was a general trend of decreasing tensile properties of YS, UTS, and EA from low temperature (−40 °C) to elevated temperature (180 °C).
(2) The effect of temperature on the HSLA BM and the HSLA-containing welded joints was similar i.e. increase in temperature decreased the strength while ductility remained the same.
(3) The DP980 BM was the only sample to show an increase in properties from room temperature (25 °C) to high temperature (180 °C). This is due to the fact that the DP980 BM exhibited minor dynamic strain ageing (DSA) behavior at 180 °C. The DP980–DP980 welded joints did not show DSA behavior due to its lower strain to failure caused by the soft zone of the DP980–DP980 welded which was dominant at 180 °C.
(4) Due to the change in shape of the DP980–DP980 tensile curve at 180 °C in comparison to the lower temperatures caused an apparent increase in hardening according to the Holloman equation which is an artifact of the model.

Acknowledgements

The authors would like to thank the Natural Sciences and Engineering Research Council of Canada (NSERC) and AUTO21 Network of Centers of Excellence for providing financial support. The financial support from International Zinc Association (IZA) and ArcelorMittal Dofasco is highly acknowledged. One of the authors (D.L. Chen) is grateful for the financial support by the Premier's Research Excellence Award (PREA), NSERC-Discovery Accelerator Supplement (DAS) Award, Canada Foundation for Innovation (CFI), and Ryerson Research Chair (RRC) program. The authors would like to thank Dr. J. Chen and Dr. Y.L. He (CANMET-Materials Technology Laboratory, Natural Resources Canada, Hamilton, Canada), Mr. E. Biro (ArcelorMittal Global Research, Hamilton, Canada), and Dr. J. Villafuerte (CenterLine (Windsor) Ltd., Windsor, Canada) for their support and helpful discussion. The assistance of Q. Li, A. Machin, J. Amankrah, and R. Churaman in performing the experiments is gratefully acknowledged.

References

[1] Murray J, King D. Oil's tipping point has passed. Nature 2012;481:433–5.
[2] Joost WJ. Reducing vehicle weight and improving U.S. energy efficiency using integrated computational materials engineering. J Mats 2012;64:1032–8.
[3] Kim HJ, Keoleian GA, Skerlos SJ. Economic assessment of greenhouse gas emissions reduction by vehicle lightweighting using aluminum and high-strength steel. J Ind Eco 2011;15:64–80.
[4] Li HZ, Sun GY, Li GY, Gong ZH, Liu DH, Li Q. On twist springback in advanced high-strength steels. Mats Des. 2011;32:3272–9.
[5] Tang L, Wang H, Li GY. Advanced high strength steel springback optimization by projection-based heuristic global search algorithm. Mats Des 2013;43:426–37.
[6] Wang WR, He CW, Zhao ZH, Wei XC. The limit drawing ratio and formability prediction of advanced high strength dual-phase steels. Mats Des 2011;32:3320–7.
[7] Kwon O, Baik SC. Manufacture and application of advanced high strength steel sheets for auto manufacture, Pohang: POSCO; p. 785–90.
[8] Xu W, Westerbaan D, Nayak SS, Chen DL, Goodwin F, Zhou Y. Tensile and fatigue properties of fiber laser welded high strength low alloy and DP980 dual-phase steel joints. Mats Des 2013;43:373–83.
[9] Farabi N, Chen DL, Zhou Y. Tensile properties and work hardening behavior of laser-welded dual-phase steel joints. J Mats Eng Perf 2012;21:222–30.
[10] Xia M, Sreenivasan N, Lawson S, Zhou Y, Tian Z. A comparative study of formability of diode laser welds in DP980 and HSLA steels. J Eng Technol 2007;129:446–52.
[11] Farabi N, Chen DL, Li J, Zhou Y, Dong SJ. Microstructure and mechanical properties of laser welded DP600 steel joints. Mater Sci Eng A 2010;527:1215–22.
[12] Farabi N, Chen DL, Zhou Y. Microstructure and mechanical properties of laser welded dissimilar DP600/DP980 dual-phase steel joints. J Alloys Comp 2011;509:982–9.
[13] Parkes D, Xu W, Westerbaan D, Nayak SS, Chen DL, Goodwin F, et al. Microstructure and fatigue properties of fiber laser welded dissimilar joints between high strength low alloy and dual phase steels. Mats Des 2013;51:665–75.
[14] Quinto L, Costa A, Miranda R, Yapp D, Kumar V, Kong CJ. Welding with high power fiber lasers – a preliminary study. Mats Des 2007;28:1231–7.
[15] Ekrami A. High temperature mechanical properties of dual phase steels. Mater Lett 2005;59:2070–4.
[16] Waterschoot T, De AK, Vandeputte S, De Cooman BC. Static strain aging phenomena in cold-rolled dual-phase steels. Metall. Mater. Trans. A 2003;34A:781–91.
[17] Ozturk F, Toros S, Kilic S. Tensile and spring-back behaviour of DP600 advanced high strength steel at warm temperatures. J Iron Steel Res 2009;16:41–6.
[18] Gündüz S. Effect of chemical composition, martensite volume fraction and tempering on tensile behaviour of steels. Mater Lett 2009;62:2381–3.
[19] Gündüz S, Tosun A. Influence of straining and ageing on the room temperature mechanical properties of dual phase steel. Mats Des 2008;29:1914–8.
[20] Molaei MJ, Ekrami A. The effect of dynamic strain aging on subsequent mechanical properties of dual-phase steels. J Mats Eng Perf 2010;19:607–10.
[21] Chen J, Young B, Uy B. Behavior of high strength structural steel at elevated temperatures. J Struct Eng 2006;132:1948–54.
[22] Dieter GE. Mechanical metallurgy. 3rd ed. New York: McGraw-Hill; 1986.
[23] Hertzberg RW. Deformation and fracture mechanics of engineering materials. 4th ed. New Jersey: John Wiley & Sons, Inc.; 1996.
[24] Hollomon JH. Tensile Deformation Trans. AIME 1945;162:268–90.
[25] Queiroz RRU, Cunha FGG, Gonzalez BM. Study of dynamic strain aging in dual phase steel. Mater Sci Eng A 2012;543:84–7.